J. Phycol. *, ***–*** (2018)

DOI: 10.1111/jpy.12766

BAFFINELLA FRIGIDUS GEN. ET SP. NOV. (BAFFINELLACEAE FAM. NOV., CRYPTOPHYCEAE) FROM BAFFIN BAY: MORPHOLOGY, PIGMENT PROFILE, PHYLOGENY, AND GROWTH RATE RESPONSE TO THREE ABIOTIC FACTORS[1]

Niels Daugbjerg,[2] *Andreas Norlin*

Marine Biological Section, Department of Biology, University of Copenhagen, Universitetsparken 4, Copenhagen Ø DK-2100, Denmark

and Connie Lovejoy

Département de Biologie, Université Laval, 1045 avenue de la Médecine, Québec, Quebec, G1V 0A6, Canada

Twenty years ago an Arctic cryptophyte was isolated from Baffin Bay and given strain number CCMP2045. Here, it was described using morphology, water- and non-water soluble pigments and nuclear-encoded SSU rDNA. The influence of temperature, salinity, and light intensity on growth rates was also examined. Microscopy revealed typical cryptophyte features but the chloroplast color was either green or red depending on the light intensity provided. Phycoerythrin (Cr-PE 566) was only produced when cells were grown under low-light conditions (5 µmol photons · m^{-2} · s^{-1}). Non-water-soluble pigments included chlorophyll *a*, c_2 and five major carotenoids. Cells measured 8.2 × 5.1 µm and a tail-like appendage gave them a comma-shape. The nucleus was located posteriorly and a horseshoe-shaped chloroplast contained a single pyrenoid. Ejectosomes of two sizes and a nucleomorph anterior to the pyrenoid were discerned in TEM. SEM revealed a slightly elevated vestibular plate in the vestibulum. The inner periplast component consisted of slightly overlapping hexagonal plates arranged in 16–20 oblique rows. Antapical plates were smaller and their shape less profound. Temperature and salinity studies revealed CCMP2045 as stenothermal and euryhaline and growth was saturated between 5 and 20 µmol photons · m^{-2} · s^{-1}. The phylogeny based on SSU rDNA showed that CCMP2045 formed a distinct clade with CCMP2293 and *Falcomonas* sp. isolated from Spain. Combining pheno- and genotypic data, the Arctic cryptophyte could not be placed in an existing family and genus and therefore Baffinellaceae fam. nov. and *Baffinella frigidus* gen. et sp. nov. were proposed.

Key index words: **Arctic flagellates; cryptophytes; growth rates; phylogeny; taxonomy; ultrastructure**

***Abbreviations*: BA, Bayesian analysis; BS, bootstrap support; Cr-PC, cryptophyte-phycocyanin; Cr-PE, cryptophyte-phycoerythrin; ML, maximum likelihood; PP, posterior probability**

Cryptophytes (=cryptomonads) are ubiquitous in marine and freshwater ecosystems worldwide and a few species have been recorded to form blooms (e.g., Laza-Martínez 2012, Šupraha et al. 2014, and references therein). However, they also reside in more extreme environments, for example, soil (Paulsen et al. 1992), snow (Javornický and Hindák 1970), and inside ikaite columns (Ikka fjord, Southwest Greenland; Kristiansen and Kristiansen 1999, N. Daugbjerg, unpub. data). The currently accepted taxonomy of Cryptomonada includes two classes: the photoautotrophic Cryptophyceae (note: *Chilomonas* is heterotrophic but this state is most likely secondarily derived) and the phagotrophic Goniomonadea. Until recently, the latter class consisted of only a single genus *Goniomonas* and some environmental sequences, but Shiratori and Ishida (2016) have described the second heterotrophic cryptomonad (*Hemiarma marina*).

The species diversity of Cryptophyceae has been studied for more than 180 years as Ehrenberg discovered the first cryptophyte (*Cryptomonas ovata*) in 1831. However, the first detailed descriptions and drawings were published 7 years later (Ehrenberg 1838). According to AlgaeBase, as of May 2018, there are 41 genera listed in the Cryptophyceae (Guiry and Guiry 2018) and of these 21 are monotypic (=53.7%).

At the biochemical level, cryptophytes possess a unique combination of pigments that include chlorophylls *a* and c_2, one of two phycobiliproteins and the cryptophyte specific carotenoid alloxanthin, alongside other common carotenoids (Hill and Rowan 1989, Cerino and Zingone 2007, Egeland 2016). The two phycobiliproteins found in cryptophytes are phycoerythrin and phycocyanin, and these have different structural configurations

[1]Received 17 April 2018. Accepted 27 June 2018. First Published Online 25 July 2018.
[2]Author for correspondence: e-mail n.daugbjerg@bio.ku.dk.
Editorial Responsibility: L. Graham (Associate Editor)

identified by their absorption peaks. Some of these configurations are unique (Hill and Rowan 1989, Novarino 2012). For each genus, only one type of phycobiliprotein is present except for *Hemiselmis* that has been shown to contain species with either Cr-PC 615 and Cr-PE 555 (Hill and Rowan 1989). As some families possess the same phycobiliprotein (Clay et al. 1999), it has been discussed if the photosynthetic pigment profile can be used to distinguish taxa at the family level (Fritsch 1935, Pringsheim 1944, Butcher 1967, Hill and Rowan 1989).

At the light microscopical level, the gross morphology of cryptophytes is somewhat similar: droplet cell shape and two flagella that emerge from the subapical end. Thus, most taxonomic differences relate to the ultrastructure of the periplast component, position of the nucleomorph, appearance of the rhizostyle, and the furrow-gullet complex (Clay et al. 1999).

In the Arctic, cryptomonads have been shown to contribute to both pelagic and sympagic communities of microalgae. They are also part of the spring bloom when the sea ice melts and nutrients are released to the open water column (Mikkelsen et al. 2008, Vallières et al. 2008, Poulin et al. 2011, Coupel et al. 2012). However, very few studies have addressed the taxonomy of Arctic cryptophytes. Recently, the species diversity of Arctic marine protists including cryptomonads was studied by molecular techniques (e.g., clone libraries and high throughput sequencing; Sørensen et al. 2012, Marquardt et al. 2016, Stecher et al. 2016). These studies have provided detailed information on operational taxonomic units, but for many of the determined ribotype sequences we have little understanding of the corresponding morphospecies.

In this study, a cryptophyte was isolated from material collected in Baffin Bay in Arctic Canada (1998), and later deposited at Provasoli-Guillard National Center for Marine Micro Algae and Microbiota in Maine, USA (Potvin and Lovejoy 2009), where it was given the strain number CCMP2045. The aim of this study was to describe this strain using a polyphasic approach, which included a morphological characterization using LM, TEM and SEM. The composition of both water and non-water-soluble pigments was analyzed to describe the profile of photosynthetic marker pigments. To infer the phylogeny of CCMP2045, the nuclear-encoded SSU rDNA sequence was compared to 50 other cryptomonads. Finally, growth rates were estimated through autecological experiments elucidating salinity and temperature tolerance limits as well as growth rates at different light intensities. Based on these results, a new genus and species *Baffinella frigidus* gen. et sp. nov. was proposed to accommodate for strain CCMP2045. The combination of morphological features and phycobiliproteins did not fit with existing families. Thus, a new family Baffinellaceae fam. nov. was also described.

MATERIALS AND METHODS

Culture. Strain CCMP2045 was isolated from a water sample collected in Baffin Bay (June 23, 1998; 76°19′15″ N, 75°49′02″ W; Fig. 1) at a depth of 11 m. A sub-culture of this strain was sent to the Marine Biological Section at University of Copenhagen where it has been kept at 4°C in L1 medium (Guillard and Hargraves 1993) with a salinity of 30 and a light:dark cycle of 16:8 h.

Microscopy. Live cells were studied using a Carl Zeiss Axio Imager.M2 with a 63× oil immersion lens. Micrographs were taken with a Zeiss AxioCam HRc digital camera (Zeiss, Oberkochen, Germany). Chlorophyll fluorescence was recorded using a Zeiss AxioCam MRc digital camera and the filter set 09 (excitation BP450-490, emission LP515). Length and width of 59 cells were measured using Zen image acquisition software from Zeiss. Means and standard deviations were calculated using IBM SPSS statistics (ver. 24, Armonk, NY, USA).

For transmission electron microscopy, 5 mL of a dense culture was fixed in 5 mL of 4% glutaraldehyde in 0.2 M cacodylate buffer containing 0.5 M sucrose for 1 h and 25 min. The fixed cells were pelleted by centrifugation and the supernatant except for 2 mL was removed. Two milliliter 0.2 M cacodylate buffer containing 0.5 M sucrose was added. After 20 min, 2 mL of the supernatant was removed and replaced with 2 mL 0.2 M cacodylate buffer without sucrose for 20 min. The mix was centrifuged at 1,201 *g* for 10 min after each of these steps. For post-fixation 2 mL of the supernatant

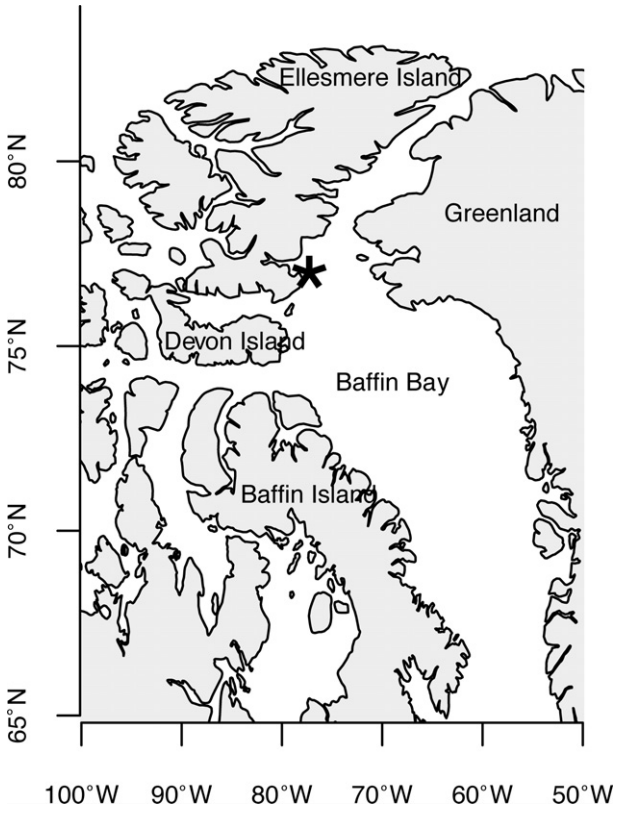

FIG. 1. Map of sampling location (*) of *Baffinella frigidus* gen. et sp. nov. in Baffin Bay.

was removed and 2 mL, consisting of 0.5 mL 4% OsO_4 and 1.5 mL 0.2 M cacodylate buffer was added for 1 h before being rinsed with 0.2 M cacodylate buffer. For dehydration, a series of ethanol was used, 20 min for each concentration (30%, 50%, 70%, 90%, and 100% in molecular sieves) with 100% in molecular sieves used twice. The pellet was rinsed twice in propylene oxide before embedding and left overnight in a mix of 1:1 propylene oxide and Spurr's resin. The next day Spurr's resin was replaced by fresh Spurr's resin for 6 h before the pellet was embedded in a cast with fresh Spurr's resin and polymerized at 70°C overnight. Thin sections were cut with a diamond knife and stained for transmission electron microscopy using uranyl acetate and lead citrate. The microscope used was a JEM 1010 electron microscope (JEOL Ltd., Tokyo, Japan) and micrographs were taken using a GATAN Orius SC1000 digital camera (Gatan, Pleasanton, CA, USA). The accelerating voltage was 80 kV.

For scanning electron microscopy, 3.5 mL of the culture was fixed in 3.5 mL 4% glutaraldehyde in 0.2 M cacodylate buffer containing 0.5 M sucrose for 1.5 h, adding 1 mL of 4% OsO_4 in seawater after 10 min. The cells were placed on a 5 μm isopore filter and rinsed in 0.2 M cacodylate buffer containing 0.5 M sucrose followed by 0.2 M cacodylate buffer containing 0.25 M sucrose and finally 0.2 M cacodylate buffer without sucrose, for 10 min each. Dehydration was done with an ethanol series (30%, 50%, 70%, 90%, and 99.9%) for 10 min each. Dehydration was finished with 100% ethanol in molecular sieves for 30 min twice before the sample was critical-point-dried. The isopore filter was attached to an aluminum stub and sputter coated with gold/palladium in a JEOL JFC-2300HR sputter coater before being observed in a JEOL JSM-6335F field emission scanning electron microscope with a secondary electron detector and running at 12 kV (JEOL Ltd.).

Pigment analyses. Extraction of the water-soluble pigment (phycobiliprotein) was based on Lawrenz et al. (2011) and briefly described here. An exponentially growing live sample (5–10 mL) was centrifuged for 5 min at 3075 g and the supernatant was removed. A volume of 2.5 mL of PBS buffer (pH 7.2 or 7.5) was added and cells were disrupted by two freeze-thaw cycles (i.e., 10 min at −80°C followed by thawing at room temperature). The extraction lasted at least 20 h at 4°C. Finally, a subsample of 1.2 mL was put in a 1.5 mL Eppendorf tube and centrifuged for 15 min at 12,202*g*. The supernatant was analyzed by scanning the spectrum between 350 and 800 nm in a Shimadzu UV180 spectrophotometer (Holm & Halby A/S, Brøndby, Denmark). Extraction of non-water-soluble pigments for HPLC were extracted in 95% methanol, and separated with a Accela 600 HPLC system (Thermo Scientific, San Jose, CA, USA) on a reverse-phase Hypersil Gold C-8 column and a solvent gradient containing methanol, aqueous pyridine, acetone, and acetonitrile (Zapata et al. 2000). An Accela PDA detector recorded chromatograms at 450 nm and pigment spectra over the wavelengths 350–800 nm. A Finnigan Surveyor FL Plus fluorescence detector with excitation of 440 nm and emission at 650 nm (optimized for Chl *a*) was also used to identify and quantitate Chl pigments. The system was calibrated by repeated injections of 30 pigment standards (Sigma Aldrich (St. Louis, MO, USA) or DHI (Hørsholm, Denmark) LAB products). ChromeQuest software was used to identify and quantitate the concentration of the pigments. The photodiode array spectrum of each peak was checked against the reference spectra of the standard or against the reference spectra in Roy et al. (2011) for pigments for which there are no standards.

Phylogenetic inference. The phylogenetic inference of CCMP2045 was based on the nuclear-encoded SSU rDNA gene, alongside the sequence of CCMP2293, which had previously been determined by Potvin and Lovejoy. The sequences were retrieved from GenBank (accession number GQ375264 and GQ375265, respectively) and added to an alignment consisting of 50 other SSU rDNA sequences of cryptomonads including 18 genera and 38 taxa identified to species. The data matrix was edited using the JALVIEW sequence editor (ver. 2.9.0b2; Waterhouse et al. 2009) following an alignment based on ClustalW as implemented in the software. The data matrix consisted of 1942 base pairs including introduced gaps. Phylogenetic reconstructions were based on BA and ML analyses. BA was performed using MrBayes (ver. 3.2.5 X64; Ronquist and Huelsenbeck 2003) on a desktop computer where 5×10^6 generations were run and a tree was sampled every 1,000 generations. The burn-in value was evaluated using the lnL value plotted as a function of generations. The lnL values converged after 101,000 generations and 101 trees were discarded, leaving 4,900 trees for generating a 50% majority-rule consensus tree in PAUP* (Swofford 2002). ML analysis was run using the PhyML software (Guindon et al. 2010) on a desktop computer with the parameter settings obtained from jModelTest (ver. 2.1.3; Darriba et al. 2012). GTR+I+G was chosen as the best fit model for the data matrix (gamma = 0.568 and p-invar = 0.464). BS were calculated from 500 replications and mapped on the tree from BA alongside the PP values.

The katablepharid *Roombia truncata* was used to root the tree as Burki et al. (2012) in a large-scale phylogenetic study had shown this taxon to form a sister to the cryptomonads.

Autecological experiments. For salinity and temperature, the autecological experiments were performed in 60 mL Nunc flasks. Triplicate flasks were placed in 24 L glass tanks containing demineralized water, circulated by an aquarium pump. A cooling system controlled by a custom made relay switched cooled water on/off and thus ensured accurate control of pre-set experimental temperatures (±0.1°C). For light experiments, the Nunc flasks were placed in a 4°C walk-in climate room, at areas where the desired light intensities were marked. Light measurements were made using a spherical PAR sensor (Walz, ULM-500; Heinz Walz GmbH, Effeltrich, Germany). The light experiments were conducted at a light:dark cycle of 16:8 h, because a shared climate room was used. pH was measured regularly (often every second day) to monitor increases due to photosynthetic activity. All experiments used a start concentration of ~1,000 cells · mL^{-1}. Samples for cell abundance measurements were collected shortly after the start of the experiments (time = t_0). Due to a linear correlation between fluorescence of chlorophyll *a* and cells · mL^{-1} when grown at the same light intensity, we converted fluorometer readings to cell abundances based on a standard curve. See Figure S1 in the Supporting Information for the standard curve used in the temperature and salinity experiments and Figure S2 in the Supporting Information for the standard curves used in the light experiments. Samples were taken every second day by pipetting 1,140 μL from each replicate into 1.5 mL Eppendorf tubes. Raw fluorescence units were measured using a Trilogy fluorometer equipped with the blue module (Trilogy, Turner Designs Instruments, Sunnyvale, CA, USA). The first replicate (A series) of each treatment was used to calculate standard curves by fixing it with Lugol's iodine (5% final concentration) and counting cell numbers using 1.0 mL Sedgewick Rafter chambers (Pyser-SGI Limited, Edenbridge, UK).

Temperature experiments. The growth rates were examined at 4.0°C, 6.0°C, 8.0°C and 10.0°C and at a salinity of 35. The light intensity was 100 μmol photons · m^{-2} · s^{-1} and the light:dark cycle 24:0 h to simulate the Arctic summer conditions.

Salinity experiments. These were conducted at salinities of 0, 5, 10, 15, 20, 25, and 30 and all at 4.0 ± 0.1°C. An

acclimation period of 3 d was included at salinities of 10 used for experiments at 0, 5, and 10, respectively; 20 used for experiments at 15 and 20, respectively; and 30 used for experiments at 25 and 30, respectively. The light setting was identical to that used in the temperature experiments. The same set of flasks and therefore the same data were used for the temperature experiment at 4°C and salinity experiment at 35.

Light experiments. These were conducted at 5, 20, 40, 60, 80, and 100 μmol photons · m^{-2} · s^{-1} at 4°C and a salinity of 30. The light:dark cycle was 16:8 h.

Calibration of growth rates. Growth rates were calculated for each replicate and the mean was based on three replicates ($n = 3$). The maximum growth rate (μ) was defined as the number of cell divisions · d^{-1} and calculated as:

$$\mu = \frac{\ln\left(\frac{N_{t2}}{N_{t1}}\right)}{t2 - t1}$$

where Nt_1 and Nt_2 were the cell abundances at the start (t_1) and end (t_2), respectively.

Statistics. Comparisons of mean growth rates by one-way ANOVA tests were performed using Graphpad Prism (ver. 7) and GraphPad Prism (ver. 6, GraphPad Software, La Jolla, CA, USA) was used to plot the data and do regression analyses.

RESULTS

We propose the following taxonomy for strain CCMP2045.

Class Cryptophyceae. Order Cryptomonadales. Chloroplasts with phycobiliprotein Cr-phycoerythrin 566 (Cr-PE III), leucoplasts present in some.

Description: Baffinellaceae Daugbjerg & Norlin fam. nov.

Furrow-gullet complex present, without stoma; nucleomorph positioned anterior to the pyrenoid; inner periplast component with partly overlapping hexagonal plates; subapical vestibular plate present; rhizostyle present.

Description: *Baffinella* Norlin & Daugbjerg gen. nov.

Two unequal flagella protruding from a furrow-gullet system in the anterior end; vestibular plate located on dorsal side of gullet; a single horseshoe-shaped chloroplast with a single pyrenoid surrounded by a starch sheet; apical end rounded and antapical end acute or bluntly rounded; hexagonal periplast plates less profound in shape at the antapical end.

Type species: *B. frigidus* sp. nov.

Etymology: from the name of the collection area, the Baffin Bay, with the Latin, feminine suffix *ella*, meaning small.

Description: *Baffinella frigidus* Norlin and Daugbjerg sp. nov.

Comma-shaped in lateral view, spherical in cross-section; dorsal side convex, ventral side more straight; live cells 5.6–11 μm long and 4.3–6.1 μm wide; gullet deep, lined with rows of large ejectosomes; pyrenoid bisected by cytoplasmic tongue; mid-dorsal band present at antapical end; nucleus in antapical end, slightly to the dorsal side; flagella inserted at one-third cell length from the apex.

Etymology: *Frigidus* from latin meaning cold, referring to its Arctic origin.

Holotype: An epon-embedded sample of strain CCMP2045 has been deposited at the National History Museum, University of Copenhagen (C), accession no. C A92087.

GenBank accession number: GQ375264, represents the nuclear-encoded SSU rDNA sequence.

Authentic culture: CCMP2045 at the Provasoli-Guillard National Center for Marine Algae and Microbiota.

Type locality: Baffin Bay (76°19′15″ N, 75°49′02″ W), Arctic Canada.

Morphology, color, and swimming behavior in LM. Cells measured 5.6–11 μm in length (average: 8.2 ± 1.2 μm, $n = 59$) and 4.3–6.1 μm in width (average: 5.1 ± 0.4 μm, $n = 59$; Fig. 2, A–J). Most cells had a comma-shaped appearance due to a small tail-like appendage in the antapical end, others were bluntly rounded (Fig. 2, A, B and D). In optical cross-section, cells were spherical (Fig. 2J). Two unequally long flagella were inserted in an apical depression (the gullet, Fig. 2, A-C, F, H and K). Rows of large ejectosomes were observed close to the gullet (Fig. 2, A, B and E). A large vacuole was present in the apical end (Fig. 2H), whereas the nucleus was located in the antapical end (Fig. 2, C and G). The structure of the periplast component surrounding the cell could be discerned in the light microscope (Fig. 2F). The single chloroplast was seen to extend in almost the full length of the cell (Fig. 2M). In cross-section, the two chloroplast lobes formed a horseshoe-shape (Fig. 2, J and L). A single pyrenoid was observed in connection with the chloroplast and it was surrounded by a starch sheet (Fig. 2I). The pyrenoid was located in the middle of the cell (Fig. 2G). A refractive crystal-like structure was present in many cells (Fig. 2, A–C). The ejectosomes discharged when cells experienced elevated heating from prolonged observations in the light microscope (Fig. 2N). Live cells swam while rotating around their longitudinal axis. Depending on the light intensity provided the color of CCMP2045 was either green or red. Live cells grown at low light (5 μmol photons · m^{-2} · s^{-1}) were red (Fig. S3, A–C in the Supporting Information), whereas cells were green if grown at light intensities ≥10 μmol photons · m^{-2} · s^{-1} (Fig. S3, D–F). Interestingly, CCMP2045 has been identified as *Rhodomonas* sp. in the culture collection at Bigelow Laboratory for Ocean Sciences (http://ncma.bigelow.org/ccmp2045); probably due to low light conditions provided.

External morphology in SEM. The apical vestibulum was part of a furrow-gullet complex (Fig. 3, A, B and D). The two flagella emerged on the right side of the gullet (Fig. 3, A and B). The vestibular plate formed a tongue-like structure located in the upper

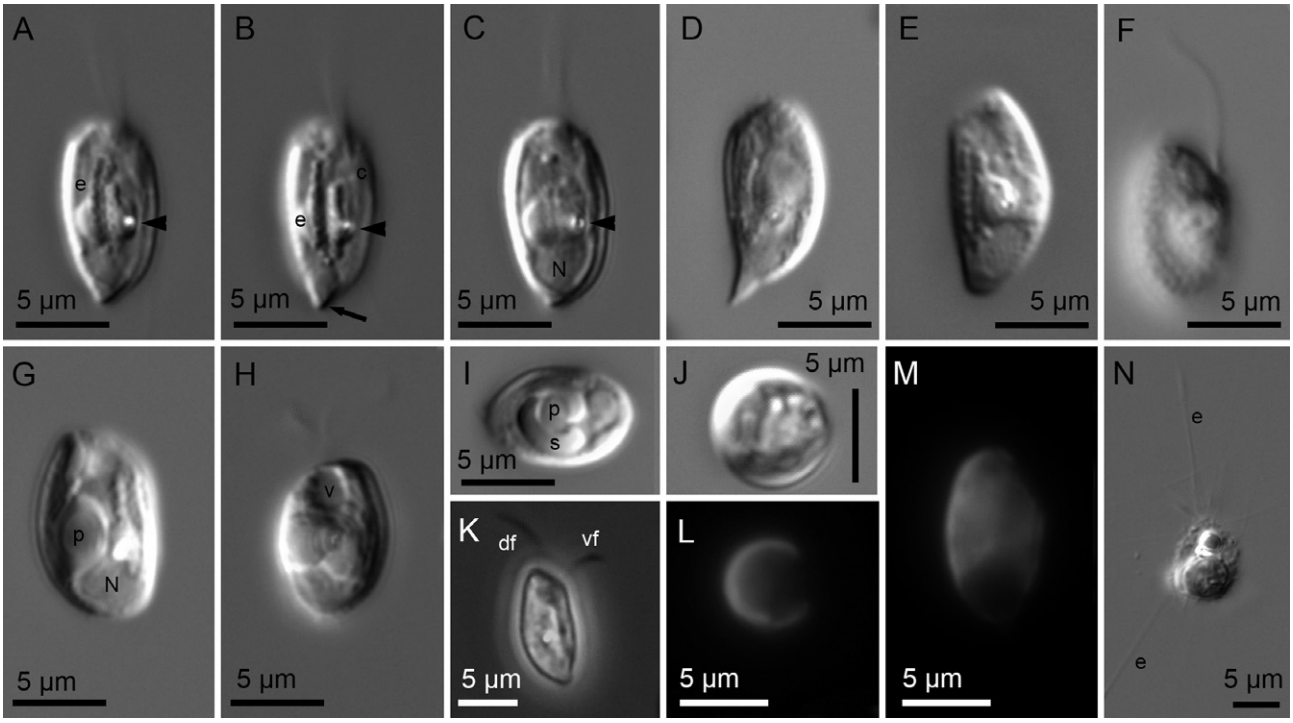

FIG. 2. Light microscopy of *Baffinella frigidus* gen. et sp. nov. grown at 100 µmol photons · m^{-2} · s^{-1}. (A–J, N) Nomarski interference contrast; (K) phase contrast; (L, M) epiflourescence. (A–C) Ventral view of cell showing gullet with large ejectosomes (e) and chloroplast (c). Note tail-like appendage (arrow, B) and nucleus (N, C) in the antapical end. Refractive vesicles are visible in A-C (arrow heads). (D–E) Lateral view showing marked comma shape in some cells (D) and bluntly rounded antapical ends in other cells (E). (F) Lateral view revealing the arrangement of periplast plates. (G) Latero-ventral view displaying posterior nucleus (N), and central pyrenoid (p). (H) Lateral view showing cell with large vacuole (v) in apical end. (I) Pyrenoid (p) surrounded by a large starch sheet (s). (J) Optical cross-section of partial chloroplast forming a horseshoe-shape. (K) Lateral-ventral view showing unequally long flagella (df, dorsal flagellum; vf, ventral flagellum). (L, M) Chloroplast in cross-section (L) and lateral view (M). Note horseshoe-shaped chloroplast in L. (N) Disintegrated cell with discharged ejectosomes (e) twice the cell in length.

part of the gullet toward the dorsal side (Fig. 3, A, B, D, F, and G). The periplast component consisted of slightly overlapping hexagonal plates arranged in 16–20 oblique rows (but see below). Each plate was ~0.6 µm in length. The periplast plates in the tail-like antapical end were smaller, the shape less profound and the number of rows (if any) could not be determined (Fig. 3, A–C). The tail-like appendage had bent in Figure 3, A, B, and D, whereas it was pointed in Figure 3C. A mid-dorsal band (sensu Hill 1991a) in the antapical end could also be discerned (Fig. 3H). A drawing illustrating the general cell outline, extent of the furrow, the vestibular plate in the vestibulum and the appearance of hexagonal periplast plates (lower part only) and how these become smaller toward the antapical end was shown in Figure 6A.

Ultrastructure in TEM. The general ultrastructure and disposition of cell organelles was illustrated in Figure 4, A and B. Large, regularly spaced ejectosome vesicles were prominent on the ventral side of the cell (Fig. 4A) and lined the inside of the gullet (Figs. 4B and 5, A and B). Small ejectosome vesicles were seen just underneath the periplast plates (Figs. 4A and 5, A–C). They were especially prominent in the antapical end where they clustered more closely compared to the rest of the cell. Discharged ejectosomes were seen to penetrate the cell perimeter (Fig. 5, D and E). The periplast was serrated giving cells a coarse appearance in sectioned material (Figs. 4A and 5A). A single chloroplast containing a pyrenoid was present on the dorsal side of the cell (Figs. 4A and 5A). The pyrenoid was surrounded by a starch sheet (Figs. 4, A, C, F and 5A) and the pyrenoid matrix itself was bisected by a cytoplasmic tongue (Figs. 4F and 5A). Flagellar basal bodies and a few features of the flagellar apparatus could be observed (Fig. 4, C–E). A 3-dimensional reconstruction was not attempted but the striated rootlet (Fig. 4, D and E), the striated rootlet microtubules (Fig. 4E) and a short, non-keeled rhizostyle (Fig. 4C) could be observed. The vestibular plate was found to be in association with the dorsal part of the gullet (Fig. 4, B and D), but a detailed understanding of the ultrastructure needs further studies. The nucleus was located in the antapical end of the cell (Fig. 4, A and B), whereas the nucleomorph was found anterior to the pyrenoid toward the apical end (Fig. 4F). The Golgi body was positioned just underneath the vestibulum

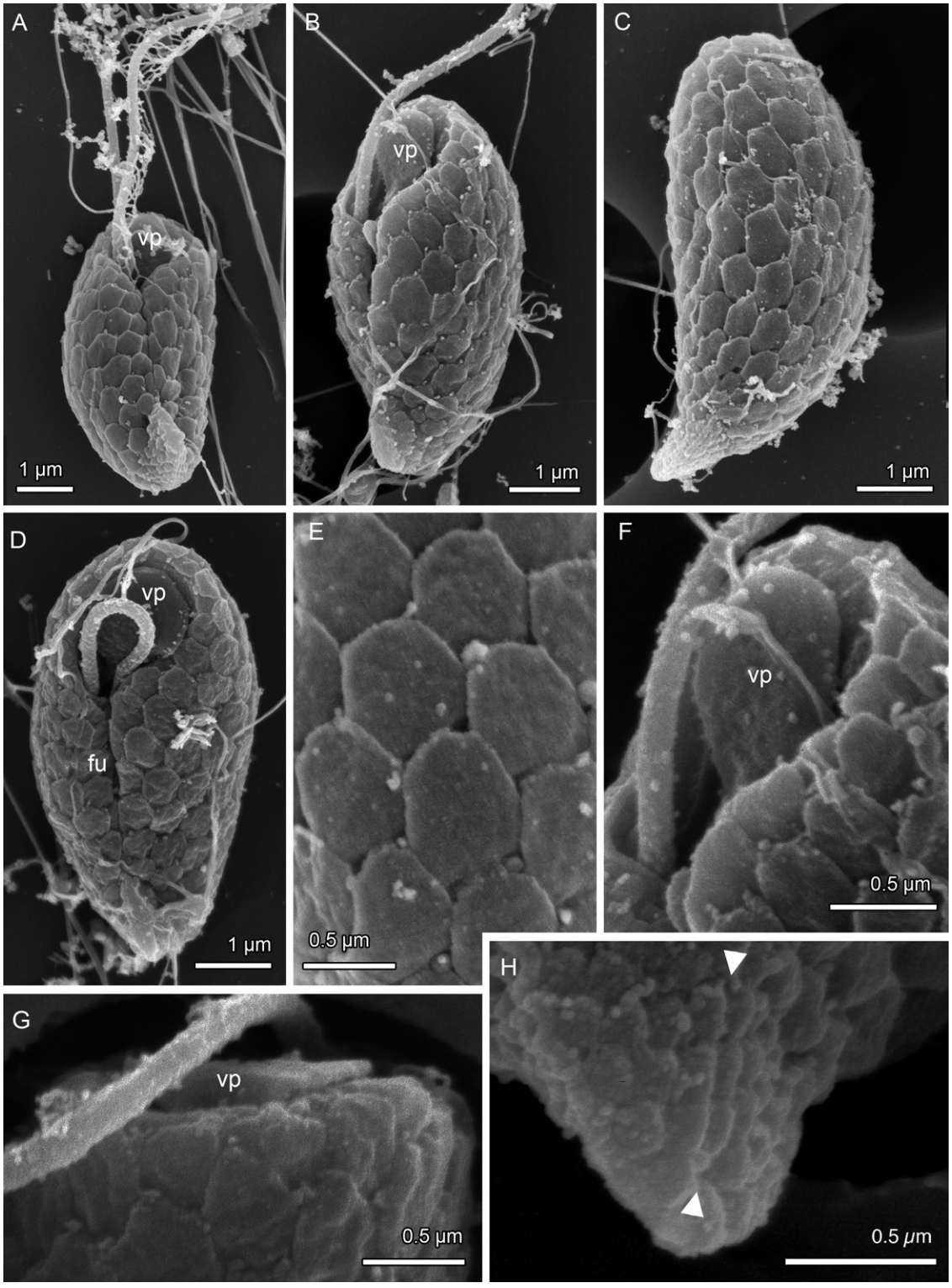

FIG. 3. Scanning electron microscopy of *Baffinella frigidus* gen. et sp. nov. illustrating external features. (A) Ventral view of cell with two flagella protruding from the right side of the furrow-gullet complex. Note discharged ejectosomes. In the gullet, the vestibular plate (vp) is seen as a tongue-like structure. (B) Ventro-lateral view with vestibular plate (vp) in the anterior part of the vestibulum. Note bending of antapical end in A and B. (C) Lateral view illustrating overlapping hexagonal periplast plates. Note that periplast plates get smaller toward antapical end. (D) Ventral view showing the furrow (fu) extending from the vestibulum. (E) High magnification the slightly overlapping periplast plates. (F) High magnification of vestibular plate (vp); same cell as in B. (G) Dorsal view of the vestibular plate (vp) raising above the apical end. (H) High magnification of tail-like appendage showing mid-dorsal band (arrow heads) and smaller periplast plates toward antapical end.

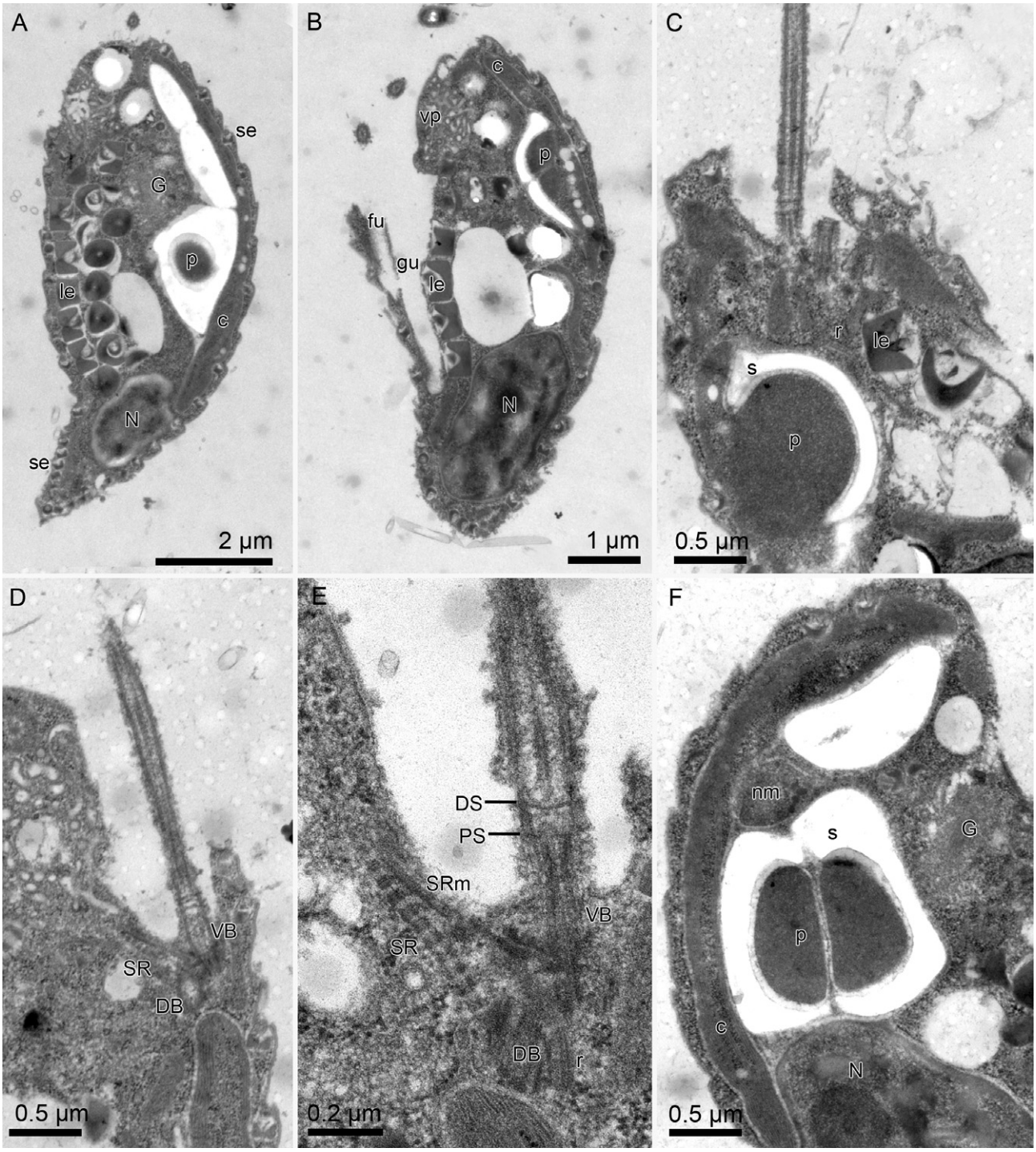

FIG. 4. Transmission electron microscopy of *Baffinella frigidus* gen. et sp. nov. (A) Lateral view showing large ejectosomes (le), posterior nucleus (N), chloroplast (c) and pyrenoid (p) with encircling starch sheet and anterio-ventrally positioned Golgi body (G). Note small ejectosomes (se) near adjoining, slightly raised anterior part of the periplast plates. (B) Lateral view showing furrow (fu) and gullet (gu) lined by large ejectosomes (le). Vestibular plate (vp) is in association with subapical part of the cell. Position of nucleus (N), pyrenoid (p), starch sheet (s) and chloroplast (c) also indicated. (C) Oblique section through apical end showing flagellar basal bodies, a short non-keeled rhizostyle (r) and pyrenoid (p) surrounded by starch (s). Large ejectosome (le). (D) Longitudinal section through apical end showing ventral (VB) and dorsal (DB) basal bodies with striated rootlet (SR). (E) Higher magnification of D showing striated rootlet (SR), striated fibrous root associated microtubular root (SRm) and distal (DS) and proximal septum (PS) of the flagellar transition zone. Ventral (VB) and dorsal (DB) basal bodies also indicated. (F) Longitudinal section showing nucleus (N) toward the antapical end, bisected pyrenoid (p) surrounded by a starch sheet (s) and anteriorly positioned nucleomorph (nm). Note also parietal chloroplast (c).

and adjacent to the basal bodies (Fig. 4F). A drawing illustrating the internal position of cell organelles was shown in Figure 6B. The single horseshoe-shaped chloroplast reaches from the apical end and down to the anterior end of the nucleus in the antapical end of the cell.

Pigment profile. The absorption spectrum of water-soluble pigments revealed a peak between 562 and 566 nm (Fig. 7). This indicated the presence of phycobiliprotein Cr-PE 566. Analysis of non-water soluble pigments revealed the presence of chlorophylls *a* and c_2 in addition to common carotenoids like alloxanthin, crocoxanthin, β,ε-carotene, lutein, and zeaxanthin (data not shown). Among the non-water-soluble pigments chlorophyll *a* and alloxanthin were present with almost equal amounts (data not shown).

Phylogeny and sequence divergence. The deepest branches of the phylogeny based on SSU rDNA were generally not supported from PP or BS values (Fig. 8). Hence, the relationship and evolutionary history among lineages, which often corresponded to families of cryptophytes, could not be discerned. However, the lineages comprising families were for the most part highly supported and in accordance with the currently accepted classification (Clay et al. 1999, Clay 2015) but with the addition of Falcomonadaceae (see Discussion). This was evident from superimposing cryptophyte families onto the phylogeny that included 18 genera. Interestingly strains CCMP2045 (studied phenotypically here) and CCMP2293 also isolated from Baffin Bay, but collected 10 April 1998, had identical SSU rDNA sequences. These strains formed an unresolved but highly supported clade (PP = 1.0 and BS = 100%) with a strain identified as *Falcomonas* sp. from North Western Spain (Raho et al. 2014). CCMP2045/CCMP2293 and the Spanish isolate of *Falcomonas* sp. only differed by 1 transition (C↔T) in the 1,686 base pairs included in the comparison. Thus, a very low sequence divergence (0.06%) was estimated between these taxa. Despite the clades comprising Geminigeraceae I and II (see Fig. 8) formed sister groups to *Baffinella* (CCMP2045, CCMP2293) and "*Falcomonas* sp." this relationship was not statistically supported (PP = 0.88, BS <50%). The heterotrophic genus *Goniomonas* (with three species included here) within the family Goniomonadaceae branched of as the first cryptomonad lineages (not monophyletic in Fig. 8). Geminigeraceae formed four highly supported but polyphyletic clades if we include *Urgorri* within this family (labeled I to IV in Fig. 8). The early divergence of the phycoerythrin containing marine *Urgorri complanatus* was not statistically supported even though it did branch of as the first autotrophic cryptophyte. The phycocyanin-containing cryptophytes seemed to form a monophyletic group but the support for this lineage was low from BA and lacking in ML bootstrap (PP = 0.88, BS <50%).

Autecology. The growth potential of *Baffinella frigidus* to changes in temperature, salinity, and light intensity was evaluated by one parameter experiments (Fig. 9, A–C). Following our experimental setup, the Artic cryptophyte CCMP2045 was able to grow (divide) at temperatures ranging from 4°C to 8°C. No growth was observed at 10°C (Fig. 9A). Significant differences in growth rates ($F_{2,6} = 415.5$; $P < 0.0001$; one-way ANOVA) were found between treatments at 4°C, 6°C, and 8°C, respectively, as indicated by lower case letters (a-c). The highest growth rate was obtained at 4°C with 0.40 divisions $\cdot$ d^{-1} and the lowest growth was obtained at 8°C with 0.15 divisions $\cdot$ d^{-1}. This equals a ≈2.7 times reduction in growth rate.

The results of the salinity one parameter experiment revealed that *Baffinella* could grow at salinities ranging from 5 to 35 (Fig. 9B). The highest growth was obtained at a salinity of 20 (0.45 divisions $\cdot$ d^{-1}), and the lowest was obtained at a salinity of 5 (0.30 divisions $\cdot$ d^{-1}). The one-way ANOVA ($F_{6,14} = 14.94$) showed three statistically different groups labelled a-c in Figure 9B and that the growth rate at a salinity of 20 was significantly higher ($P < 0.05$) compared to that at salinities of 5, 10, and 30, but not significantly higher ($P > 0.51$) compared to salinities at 15, 25, and 35. The growth rate at a salinity of 5 was significantly lower ($P < 0.01$) compared to all other salinities (Fig. 9B).

The light experiments demonstrated that the growth rates were not significantly different when grown at 20 μmol photons $\cdot$ m^{-2} $\cdot$ s^{-1} and above (Fig. 9C). Here, the growth rate was 0.39 divisions $\cdot$ d^{-1}, whereas the growth rate at 5 μmol photons $\cdot$ m^{-2} $\cdot$ s^{-1} was significantly ($P < 0.001$) lower and only reached 0.17 divisions $\cdot$ d^{-1}. The one-way ANOVA ($F_{5,12} = 130.7$) showed two groups, thus, one with 5 μmol photons $\cdot$ m^{-2} $\cdot$ s^{-1} and the other containing the rest of the light intensities (labelled a and b, respectively, in Fig. 9C). Hence, *Baffinella frigidus* was light saturated a 20 μmol photons $\cdot$ m^{-2} $\cdot$ s^{-1} and may be even at slightly lower levels but this has to be studied in more detail.

For all autecological experiments, the growth terminated when the pH reached 8.6–9 (data not shown). Graphs for all autecological experiments showing cell abundances as a function of time are provided as supplementary Figures S4–S6 in the Supporting Information.

DISCUSSION

To the best of our knowledge, this is the first marine cryptophyte described from high Arctic waters. The description was based on a polyphasic approach that included pheno- and genotypic characters in addition to exploring the potential growth rates at different temperatures, salinities and light intensities.

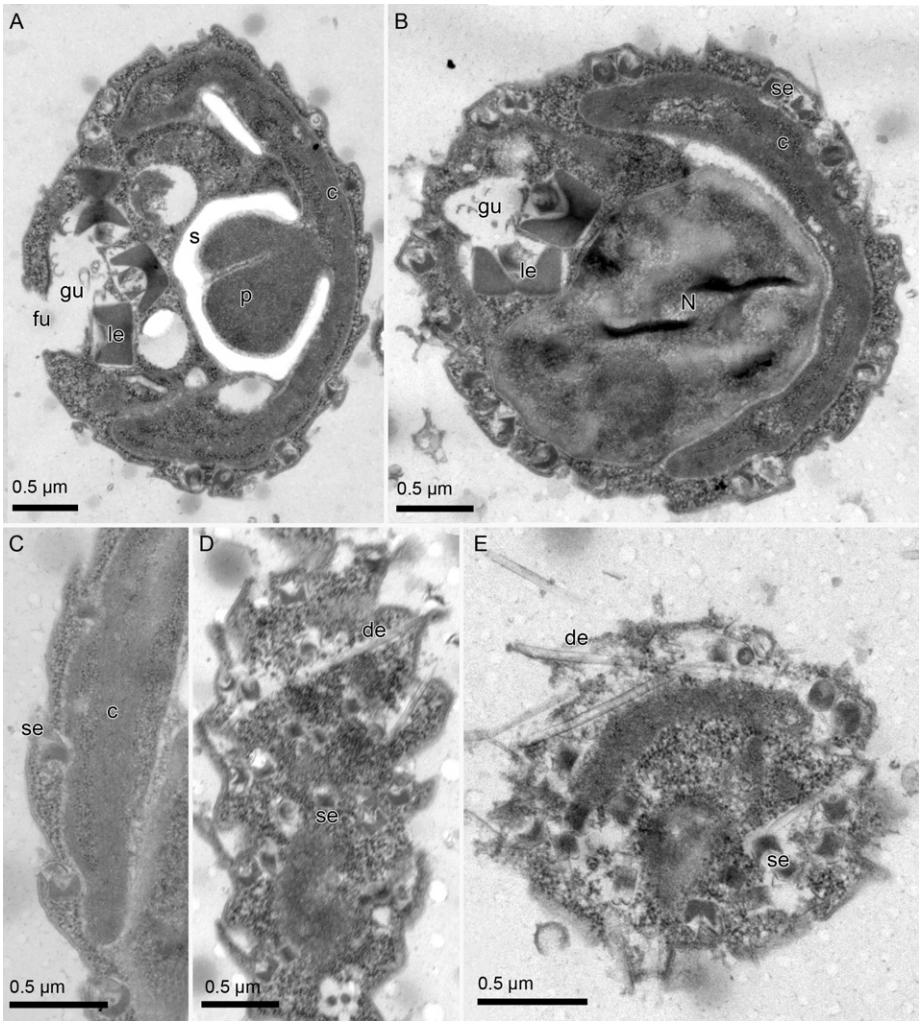

FIG. 5. Transmission electron microscopy of *Baffinella frigidus* gen. et sp. nov. (A) Cross-section at the level of the bisected pyrenoid (p) enclosed by starch (s). The furrow (fu) and gullet (gu) complex also visible. Rows of large ejectosomes (le) located near the gullet. Note also single, parietal chloroplast (c). (B) Posterior part of cell showing gullet (gu), nucleus (N), large (le), and small (se) ejectosomes and horseshoe-shaped chloroplast (c). (C) Serrated outline of cell exterior is due to overlapping periplast plates. Chloroplast (c) separated from cell membrane by small somewhat evenly distributed small ejectosomes (se). (D, E) Serrated outline of cell exterior and cell body traversed by discharged ejectosomes (de). Numerous small sized, non-discharged ejectosomes (se) also present.

Taxonomy and phylogeny. The taxonomy of the Cryptophyceae has been based on cell size and shape, furrow-gullet complex, inner, and outer composition of the periplast components, position of the nucleomorph and the type of biliprotein (either red or blue-green water-soluble pigments; for example, Clay et al. 1999, Novarino 2012). *Baffinella frigidus* possessed morphological and biochemical features typical of cryptophytes but also some uncommon characters. Table 1 provides a list of characters and character states currently used to distinguish both marine and freshwater cryptophyte genera. The phylogenetic inference based on SSU rDNA supported the monophyletic status of autotrophic families Baffinellaceae, Falcomonadaceae (see later), Hemiselmidaceae, Pyrenomonadaceae, and Cryptomonadaceae, whereas families Chroomonadaceae (with two distinct lineages) and Geminigeraceae (with distinct four lineages if accepting *Urgorri* as a member) were not. Hence, additional studies are needed to fully understand the taxonomy of the latter two families of Cryptophyceae.

Vestibular plate. Baffinella had no single synapomorphic trait that separated it from other cryptophytes. Rather it had a unique combination of characters that made it distinct. As can be seen from Table 1 this applies to the majority of cryptophytes. One of the more unusual features of *Baffinella* was the vestibular plate in the vestibulum. However, a vestibular plate has also been observed in two other marine genera *Falcomonas* and *Proteomonas*. Following the phylogenetic reconstruction based on the single gene tree, cryptophytes possessing vestibular

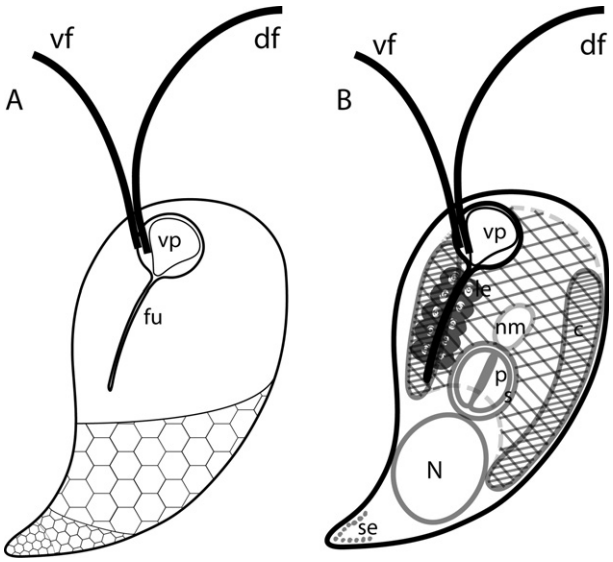

FIG. 6. Schematic illustrations of *Baffinella frigidus* gen. et sp. nov. in ventro-lateral view. (A) Illustration showing different sizes of the oblique rows of hexagonal periplast plates and length of furrow (fu). The vestibular plate (vp) and the ventral (vf) and dorsal flagella (df) are also shown. (B) Illustration showing position of major cell organelles: nucleus (N), bisected pyrenoid (p), starch sheet (s), nucleomorph (nm), large (le), and small (se) ejectosomes and chloroplast (c). The slightly overlapping periplast plates and serrated outline of the cell exterior is not shown.

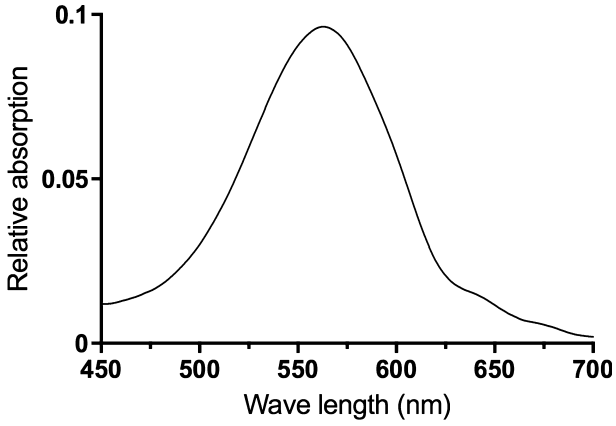

FIG. 7. Absorbance spectrum of the water-soluble pigments of *Baffinella frigidus* gen. et sp. nov. showing a peak at 566 nm, revealing the presence of Cr-PE 566.

plates are not closely related and therefore this feature appears to have developed independently at least three times (or alternatively lost multiple times). Hill and Wetherbee (1986) speculated on the function of the vestibular plate in *Proteomonas sulcata*, and suggested that it could be a specialized receptive area similar to a mating structure seen in some gametes of green algae. In this context, it is interesting that *Proteomonas* contains a haploid and diploid stage each with different morphotypes. This strongly implies sexual reproduction, but transition between stages in the heteromorphic life cycle of *P. sulcata* has not been observed (Hill and Wetherbee 1986). Potvin and Lovejoy (2009) determined the relative amounts of DNA in cells of strains CCMP2045 and CCMP2293. They found that CCMP2045 had twice the amount of DNA compared to CCMP2293. Thus, CCMP2045 likely represents the diplo- and CCMP2293 the haplomorph stages of *Baffinella*. The two strains had identical SSU rDNA sequences. Unfortunately, the morphology of strain CCMP2293 has not yet been studied in detail but we hypothesize that *B. frigidus* represents the second marine cryptophyte with a dimorph stage. Future studies will also have to show if a dimorphic stage is characteristic of *Falcomonas daucoides*. Thus, at present two out of three cryptophytes with haplo- and diploid stages indicative of sexual reproduction possess vestibular plates. This adds support to the function of the vestibular plate taken part in sexual reproduction. In the freshwater genus *Cryptomonas*, dimorphic species have also been described (Hoef-Emden and Melkonian 2003). However, here sexual reproduction takes place without a vestibular plate.

Furrow-gullet complex. The morphology and extension of the gullet-furrow complex has been emphasized as a diagnostic feature in cryptophyte taxonomy (e.g., Butcher 1967, Clay et al. 1999). Kugrens et al. (1986) listed five different types. However, as it can be seen in Table 1 different types of furrow-gullet complexes are present in the same family (Geminigeraceae and Pyrenomonadaceae) making it difficult to use as a diagnostic character at this taxonomic level. Rather the evolution of the furrow-gullet complex appears little constrained and to be identified by character reversals. *Baffinella* shares a furrow-gullet complex with the marine genus *Geraminigera* and the freshwater genera *Pyrenomonas* and *Cryptomonas*. Like *Falcomonas*, most other cryptophytes possess only a furrow.

Inner periplast components. The shape and appearance of this character is also considered important in delineation of cryptophyte genera (Clay et al. 1999). Periplast plates with a hexagonal outline as in *Baffinella* also occurs in a number of unrelated genera of both marine (*Falcomonas*, *Proteomonas* and *Rhinomonas*) and freshwater (*Chroomonas*, *Komma* and *Hemiselmis*) cryptophytes. Based on the tree topology in Figure 8, the evolutionary history of the shape of the inner periplast components was suggested to involve independent origins.

Cell shape and posterior end. The marked comma shape of some *Baffinella frigidus* cells was due to an acute posterior. Under the microscope other cells were bluntly rounded. The reason for the different outline of the posterior end is unknown. In SEM, the tail-like appendage was sometimes seen to bend completely backwards, which indicated a high degree of flexibility. A few other cryptophytes have also been described with an acute posterior end (e.g., *F. daucoides*,

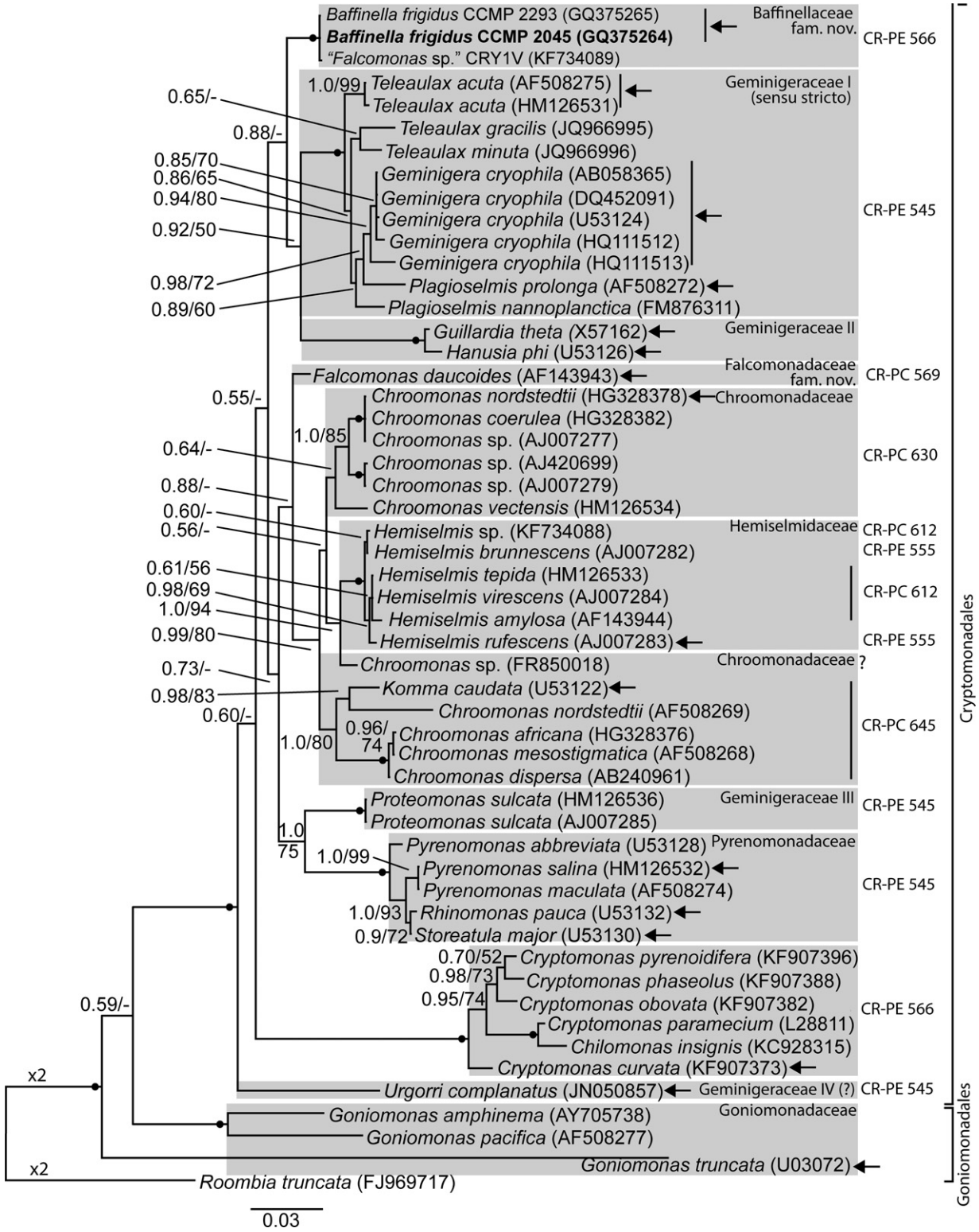

FIG. 8. Phylogenetic tree of cryptophytes (18 genera) revealing the position of *Baffinella frigidus* gen. et sp. nov. (CCMP2045, marked in bold face) based on nuclear encoded SSU rDNA gene sequences. *Roombia truncata* (Katablepharidea) formed the outgroup taxon. The tree topology was based on BA and the robustness of clades was evaluated by PP from BA and BS values from ML analyses (500 replications). Support values are indicated at internodes (PP values ≥0.5/BS values ≥50%). Maximum values (PP = 1 and BS = 100%) are indicted by filled circles. Currently, accepted families are superimposed on the tree and indicated by gray boxes. The types of cryptophyte biliproteins (either Cr-PE (phycoerythrin) or Cr-PC (phycocyanin) are indicated for each taxon. Type species are indicated by arrows. Branch lengths are proportional to the number of character changes.

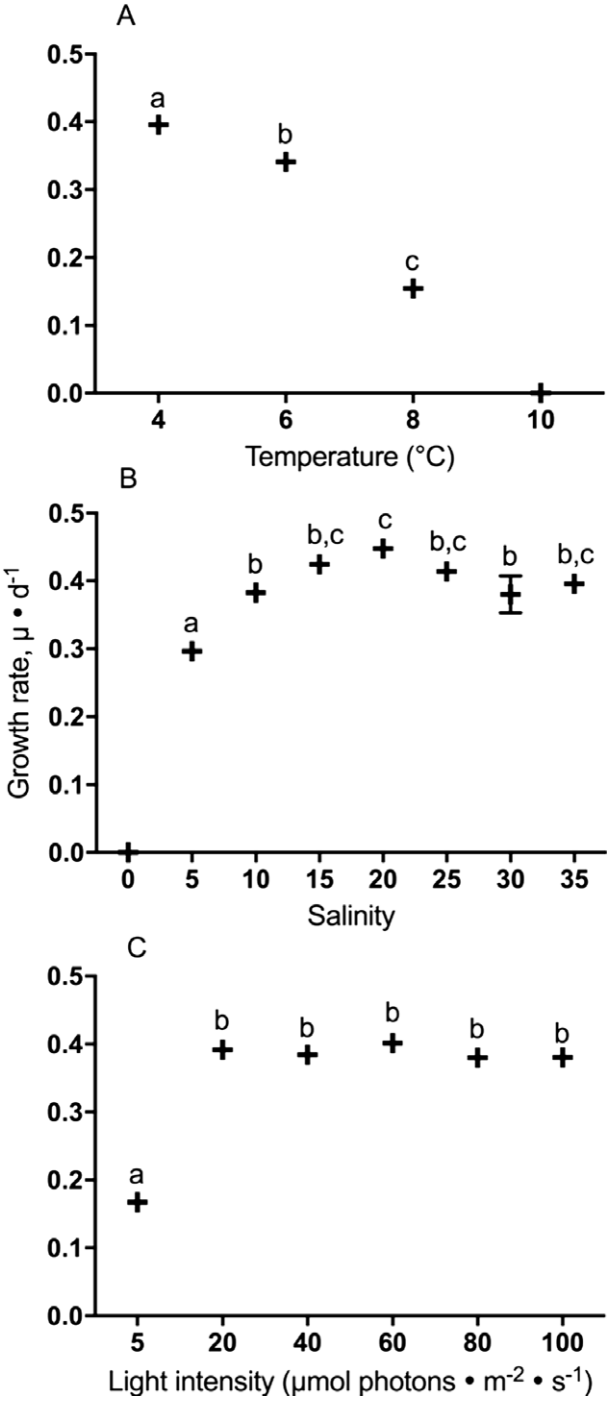

FIG. 9. Abiotic factors (temperature, salinity and light intensity) affecting the growth rate of *Baffinella frigidus* gen. et sp. nov. (A) Growth rates as a function of temperatures ranging from 4°C to 10°C. (B) Growth rates as a function of salinities ranging from 5 to 35. (C) Growth rates as a function of light intensities ranging from 5 to 100 μmol photons · m^{-2} · s^{-1}. Identical letters in each of the three figures mark non-significant results from one-way ANOVA analyses.

Komma caudata, *Plagioselmis prolonga*, *Teleaulax* spp.). The adaptive value (if any) of the posterior tail-like appendage remains obscure. Again, there is no close relationship between these taxa indicating multiple origins of a similar cell outline in cryptophytes.

Position of nucleomorph. In *Baffinella*, the nucleomorph was positioned anterior to the pyrenoid. A similar position of the pyrenoid is also seen in *Falcomonas*, *Teleaulax*, *Guillardia*, and *Chroomonas*. These taxa represent four families and contrary to Hoef-Emden et al. (2002) we do not find that this character was completely congruent with the tree topology in our phylogenetic analyses. Rather, the position of the nucleomorph seemed to have had a complex evolutionary history.

Phylogeny of Baffinella frigidus. *Baffinella frigidus* was related to strain CRY1V from NW Spain (Ria de Vigo) identified as *Falcomonas* sp. using morphology only (Raho et al. 2014). Only a single nucleotide substitution difference separated the two taxa when comparing their SSU rDNA sequences (1,686 base pairs). *Falcomonas* sp. was only distantly related to *F. daucoides* identified using electron microscopy and phycobilin spectroanalysis (Hill 1991a, Clay and Kugrens 1999). The Spanish strain was grown at 18.5°C, whereas it was shown here that *B. frigidus* cannot survive at temperatures above 10°C. Despite high sequence similarity, the difference in temperature preferences indicates that the two strains represent markedly different ecotypes. Further studies of CRY1V are needed before the taxonomy of this strain can be completed understood.

Why a new family and genus? From the list of characters and their states (Table 1) CCMP2045 did not fit into any of the families in the cryptophyte classification schemes suggested by Clay et al. (1999) and Clay (2015). Due to the presence of Cr-PE 566, *Baffinella frigidus* belongs to the order Cryptomonadales. This order has one family, the Cryptomonadaceae but because the disposition of the nucleomorph (anterior to pyrenoid in *Baffinella* and between the pyrenoid and the nucleus in Cryptomonadaceae), morphology of the pyrenoid matrix (bisected in *Baffinella* and not traversed in Cryptomonadaceae), occurrence of vestibular plate (present in *Baffinella* and absent in Cryptomonadaceae) it did not allow for an inclusion of *Baffinella* into the Cryptomonadaceae. These differences were considered sufficient for the establishment of a new family. Similarly, no description of an existing cryptophyte genus completely matched the features of *Baffinella* explaining the need for erecting a new genus. This was also supported by the distinct lineage containing *Baffinella* in the SSU rDNA tree (Fig. 8).

Light dependent chloroplast color. When grown in Nunc flasks, the color of the chloroplast in *Baffinella* either appeared green or red depending on the light intensity provided. Hence, at light levels ≥10 μmol photons · m^{-2} · s^{-1}, the chloroplast was green; whereas at low light (5 μmol photons · m^{-2} · s^{-1}), it was red. This was also clearly

TABLE 1. Characters and characters states used to delineate cryptophyte genera. Their taxonomy into families is also included. Modified from Clay et al. (1999), Clay (2015), Hill (1991b), Hill and Wetherbee (1986, 1988), Hoef-Emden and Archibald (2016) and Laza-Martínez (2012).

Family	Genus	Furrow-gullet complex	Shape of inner periplast component	Rhizostyle	Number, position of nucleomorph	Type of biliprotein	Number, morphology of pyrenoid	Chloroplast number	Vestibular ligule	Vestibular plate	Eyespot	Habitat
Baffinellaceae fam. nov.	*Baffinella* gen. nov.	Furrow and gullet	Hexagonal	Non-keeled	1, anterior to pyrenoid	PE 566	1, bisected by periplastidial cytoplasmic tongue	1	No	Yes	No	Marine
Geminigeraceae	*Teleaulax*	Furrow only	Sheet	Keeled	1, anterior to pyrenoid	PE 545	1, not traversed	1	No	No	No	Marine
	Geminigera	Furrow and gullet	Sheet	Keeled	1, invagination in nucleus	PE 545	2, not traversed by thylakoids	1	No	No	No	Marine
	Plagioselmis	Furrow only	Hexagonal	Non-keeled	1, between pyrenoid and nucleus	PE 545	1, not traversed	1	No	No	No	Freshwater, Marine
	Guillardia	Gullet only	Irregular sheet-like plates	Keeled	1, anterior to pyrenoid	PE 545	1, not traversed	1	No	No	No	Marine
	Hanusia	Furrow only	Sheet	Keeled	1, between pyrenoid and nucleus	PE 545	1, not traversed	1	No	No	No	Marine
	Proteomonas	Furrow only	Hexagonal (1n), sheet (2n)	Non-keeled (1n), keeled (2n)	1, between pyrenoid and nucleous	PE 545	1, not traversed	1	No	Yes	No	Marine
	Urgorri[a] (campylomorph)	Furrow only	Inner sheet (?)	Keeled	1, between pyrenoid and nucleus	PE 545	3, not traversed	1	No	No	Yes	Marine
Falcomonadaceae fam. nov.	*Falcomonas*	Furrow only	Hexagonal	None	1, anterior to pyrenoid	PC 569	1, bisected by periplastidial cytoplasmic tongue	1	No	Yes	No	Marine
Chroomonadaceae	*Chroomonas*	Gullet only, sometimes branched	Rectangular or hexagonal	None	1, anterior to pyrenoid	PC 630 or PC645	1–2, traversed by thylakoids	1–2	No	No	Yes, but not all	Freshwater
	Komma	Gullet only	Rectangular, hexagonal	None	Between pyrenoid and nucleus	PC 645	1, not traversed	1	No	No	No	Freshwater
Pyrenomonadaceae	*Pyrenomonas*	Furrow and gullet	Rectangular	Keeled	1, in pyrenoid matrix	PE 545	1, not traversed	1	No	No	No	Freshwater
	Rhinomonas	Gullet only	Hexagonal	None	1, in pyrenoid matrix	PE 545	1, not traversed	1	No	No	No	Marine
	Storeatula	Gullet only	Inner sheet	Keeled	1, in pyrenoid matrix	PE 545	1, not traversed	1	No	No	No	Freshwater
Cryptomonadaceae	*Cryptomonas*	Furrow and gullet	Fibrous	Non-keeled	2, between pyrenoids and nucleus	PE 566 or leucoplast	0, 2 (4), not traversed	2	Some	No	No	Freshwater
Hemiselmidaceae	*Hemiselmis*	Gullet only	Hexagonal	None	1, between pyrenoid and nucleus	Red species: PE 555, PE 577; Blue-green species: PC 615, PC630	1, round and traversed by thylakoids	1	No	No	Yes?	Freshwater

[a]*Urgorri* is provisionally placed in the family Geminigeraceae.

seen in the light microscope and documented in Figure S3. Thus, the color of *B. frigidus* was rather cryptic. Analysis of water soluble pigments revealed a clear peak around 566 nm indicating the presence of phycoerythrin Cr-PE 566 when grown at low light. Cells grown at 20–100 μmol photons $\cdot$ m^{-2} $\cdot$ s^{-1} showed no peaks corresponding to a biliprotein (data not shown). A study on a species of *Rhodomonas* (now *Pyrenomonas*) by Chaloub et al. (2015) showed similarly that the amount of phycoerythrin increased when cells were grown at low light levels (<15 μmol photons $\cdot$ m^{-2} $\cdot$ s^{-1}) compared to 50 and 150 μmol photons $\cdot$ m^{-2} $\cdot$ s^{-1}. In addition, Chaloub et al. (2015) showed that the phycoerythrin content decreased in *Rhodomonas* cells approaching the stationary phase. Color changes have also been observed in other cryptophytes. Butcher (1967) and Pringsheim (1968) both noted that when cultures were starved the cell color changed. In this study, cells were probably not starved in terms of nutrient supply but rather with respect to available light. Light dependent presence of phycobiliproteins should be taken into account when describing the color of chloroplasts in cryptophytes.

Taxonomy of Falcomonas. On the basis of phylogenetic analyses and the comparative study of phenotypic characters, we propose here to formally describe the family Falcomonadaceae. This taxon was first suggested by Clay and Kugrens (1999), but it was illegitimate according to IBCN article 39.1 (no diagnosis or description provided).

Description: Falcomonadaceae fam. nov. Daugbjerg

Furrow only; vestibular plate present; nucleomorph anterior to pyrenoid; pyrenoid traversed by cytoplasmic tongue; hexagonal inner periplast plates; rhizostyle absent.

Currently only one genus with one species in the family: *Falcomonas daucoides* Hill

Autecology. On the basis of the results of the autecological experiments, we concluded that *Baffinella frigidus* was stenothermal and euryhaline. However, the lower temperature and upper salinity ranges where cells can longer to divide were not determined. Yet, it appears that *B. frigidus* is well adapted to the environmental settings of Baffin Bay, where the subsurface water temperature rarely gets above 8°C and the salinity lower than 5–10 despite seasonal melting of sea ice. We are unaware of other autecological studies addressing the potential growth of Arctic marine cryptophytes when exposing them to changes in environmental factors. Most studies that report on growth rates of Arctic microalgae deal with diatoms and green algal flagellates. For diatoms (e.g., *Fragilariopsis*), the growth rates varied between 0.3 and 0.9 divisions $\cdot$ d^{-1} (Hegseth 1992, Pančić et al. 2015). For the green algal genus *Pyramimonas*, the growth rates were in the range of 0.32 to 0.55 division $\cdot$ d^{-1} at low temperatures (<9°C–10°C) and a suite of salinities (5–30; Daugbjerg and Moestrup 1992a,b, Salmansen and Daugbjerg, unpub. data). For the picoflagellate *Micromonas* sp., the maximum growth rate was found to be 0.55 divisions $\cdot$ d^{-1} at 8°C, when light was not a limiting factor (Lovejoy et al. 2007). Thus, comparing the rates of *Baffinella* to those of other Arctic microalgae revealed that it is grows slightly slower than *Pyramimonas* spp. and *Micromonas* sp. and is in the mid-range compared to the pennate diatom *Fragilariopsis*. A single study has addressed the growth rate of a freshwater cryptophyte (*Rhodomonas* sp.) from the Arctic and provided in situ rates in an ice-covered lake to range from 0.07 to 0.18 divisions $\cdot$ d^{-1} (Vehmaa and Salonen 2009).

Future studies. Additional studies should address the presumable haplomorph of *Baffinella frigidus* (CCMP2293) and focus on ultrastructure of the inner periplast component, the vestibular plate, the position of the nucleomorph and type of phycobiliprotein. In addition, a more complete characterization is needed for a proper identification of strain CRY1V from NW Spain. We doubt that it is a species of *Falcomonas* and it should be determined if it represents an ecotype of *B. frigidus*. Temperature is an environmental factor that clearly distinguishes the unique ecological niches of CCMP2045 and CRY1V, which otherwise seem to form a single phylospecies. The growth rate of *B. frigidus* when provided light intensities between 5 and 20 μmol photons $\cdot$ m^{-2} $\cdot$ s^{-1} should be investigated to better understand when the chloroplast changes color due to disappearance of Cr-PE 566. Despite this first polyphasic study, our understanding of the species diversity of Arctic marine cryptophytes is still in its infancy. Thus, future studies should address the alpha taxonomy of these small sized flagellates from the vast regions of the Arctic.

We thank Lis Munk Frederiksen, Ayoe Lücheu and Øjvind Moestrup for technical assistance. We thank Marie Jose Martineau and W.F Vincent for pigment data. ND thanks the Carlsberg Foundation (2012-01-0509) and Brødrene Hartmanns Fond (A22920) for equipment grants. We also thank reviewers for their constructive comments on an earlier version of the manuscript.

Burki, F., Okamoto, N., Pombert, J.-F. & Keeling, P. J. 2012. The evolutionary history of haptophytes and cryptophytes: phylogenomic evidence for separate origins. *Proc. R. Soc. B Biol. Sci.* 279:2246–54.

Butcher, R. W. 1967. An introductory account of the smaller algae of British coastal waters. Part IV: Cryptophyceae. *Fish. Investig*, London, Ser. IV, 54 pp.

Cerino, F. & Zingone, A. 2007. Decrypting cryptomonads: a challenge for molecular taxonomy. *In* Brodie, J. & Lewis, J. [Eds] *Unravelling the Algae: The Past, Present, and Future of Algal Systematics*. CRC Press, Boca Raton, Florida, pp. 197–214.

Chaloub, R. M., Motta, N. M. S., de Araujo, S. P., de Aguiar, P. F. & da Silva, A. F. 2015. Combined effects of irradiance, temperature and nitrate concentration on phycoerythrin content in the microalga *Rhodomonas* sp. (Cryptophyceae). *Algal Res.* 8:89–94.

Clay, B. L. 2015. Cryptomonads. *In* Wehr, J., Sheath, R. & Kociolek, J. P. [Eds.] *Freshwater Algae of North America*. Elsevier Inc, London, Waltham, pp. 809–50.

Clay, B. L. & Kugrens, P. 1999. Characterization of *Hemiselmis amylosa* sp. nov. and phylogenetic placement of the blue-green cryptomonads *H. amylosa* and *Falcomonas daucoides*. *Protist* 150:297–310.

Clay, B. L., Kugrens, P. & Lee, R. E. 1999. A revised classification of Cryptophyta. *Bot. J. Linn. Soc.* 131:131–51.

Coupel, P., Jin, H. Y., Joo, M., Horner, R., Bouvet, H. A., Sicre, M. A., Gascard, J. C. et al. 2012. Phytoplankton distribution in unusually low sea ice cover over the Pacific Arctic. *Biogeosciences* 9:4835–50.

Darriba, D., Taboada, G. L., Doallo, R. & Posada, D. 2012. jModelTest 2: more models, new heuristics and parallel computing. *Nat. Methods* 9:772.

Daugbjerg, N. & Moestrup, Ø. 1992a. Fine structure of *Pyramimonas cyclotreta* sp. nov. (Prasinophyceae) from Northern Foxe Basin, Arctic Canada, with some observations on growth rates. *Eur. J. Protistol.* 28:288–98.

Daugbjerg, N. & Moestrup, Ø. 1992b. Ultrastructure of *Pyramimonas cyrtoptera* sp. nov. (Prasinophyceae), a sixteen-flagellate species from Northern Foxe Basin, Arctic Canada, including observations on growth rates. *Can. J. Botany* 70:1259–73.

Egeland, E. S. 2016. Carotenoids. *In* Borowitzka, M. A., Beardall, J. & Raven, J. A. [Eds.] *The Physiology of Microalgae*. Springer International Publishing, Switzerland, pp. 507–63.

Ehrenberg, C. G. 1831. *Animalia Evertebrata exclusis Insectis. Series Prima cum Tabularum Decade Prima*. Berolini ex Officina Academica, Berlin, pp. 1–126.

Ehrenberg, C. G. 1838. *Die Infusionsthierschen als volkommene Organismen. Ein Blick in das tiefere organische Leben der Natur*. Leopold Voss, Leipzig. 548 pp. + atlas.

Fritsch, F. E. 1935. Class V. Cryptophyceae. *In* Fritsch, F. E. [Ed.] *The Structure and Reproduction of the Algae. Volume 1*. 1965 repri. Cambridge University Press, London and New York, pp. 652–64.

Guillard, R. R. L. & Hargraves, P. E. 1993. *Stichochrysis immobilis* is a diatom, not a chrysophyte. *Phycologia* 32:234–6.

Guindon, S., Dufayard, J. F., Lefort, V., Anisimova, M., Hordijk, W. & Gascuel, O. 2010. New algorithms and methods to estimate maximum-likelihood phylogenies: assessing the performance of PhyML 3.0. *Syst. Biol.* 59:307–21.

Guiry, M. D. & Guiry, G. M. 2018. AlgaeBase. World-wide electronic publication, National University of Ireland, Galway. Available at: http://www.algaebase.org (last accessed March 2018).

Hegseth, E. N. 1992. Sub-ice algal assemblages of the Barents Sea: species composition, chemical composition and growth rates. *Polar Biol.* 12:485–96.

Hill, D. R. A. 1991a. *Chroomonas* and other blue green cryptomonads. *J. Phycol.* 27:133–45.

Hill, D. R. A. 1991b. A revised circumscription of *Cryptomonas* (Crytophyceae) based on examintation of Australian strains. *Phycologia* 30:170–88.

Hill, D. R. A. & Rowan, K. S. 1989. The biliproteins of the Cryptophyceae. *Phycologia* 28:455–63.

Hill, D. R. A. & Wetherbee, R. 1986. *Proteomonas sulcata* gen. et sp. nov. (Cryptophyceae), a cryptomonad with two morphologically distinct and alternating forms. *Phycologia* 25:521–43.

Hill, D. R. A. & Wetherbee, R. 1988. The structure and taxonomy of *Rhinomonas pauca* gen. et sp. nov. (Cryptophyceae). *Phycologia* 27:355–65.

Hoef-Emden, K. & Archibald, J. M. 2016. Cryptophyta (Cryptomonads). *In* Archibald, J. M., Simpson, A. G. B., Slamovits, C. H., Margulis, L., Melkonian, M., Chapman, D. J. & Corliss, J. O. [Eds.]. *Handbook of the Protists*. Springer International Publishing, Cham, Switzerland, 41 pp.

Hoef-Emden, K., Marin, B. & Melkonian, M. 2002. Nuclear and nucleomorph SSU rDNA phylogeny in the Cryptophyta and the evolution of cryptophyte diversity. *J. Mol. Evol.* 55:161–179.

Hoef-Emden, K. & Melkonian, M. 2003. Revision of the genus *Cryptomonas* (Cryptophyceae): a combination of molecular phylogeny and morphology provides insights into a long-hidden dimorphism. *Protist* 154:371–409.

Javornický, P. & Hindák, F. 1970. *Cryptomonas frigoris* spec. nova (Cryptophyceae), the new cyst-forming flagellate from the snow of the High Tatras. *Biològia (Bratislava)* 25:241–50.

Kristiansen, J. & Kristiansen, A. 1999. A new species of *Chroomonas* (Cryptophyceae) living inside the submarine ikaite columns in the Ikkafjord, Southwest Greenland, with remarks on its ultrastructure and ecology. *Nord. J. Bot.* 19:747–58.

Kugrens, P., Lee, R. E. & Andersen, R. A. 1986. Cell form and surface patterns in *Chroomonas* and *Cryptomonas* cells (Cryptophyta) as revealed by scanning electron microscopy. *J. Phycol.* 22:512–22.

Lawrenz, E., Fedewa, E. J. & Richardson, T. L. 2011. Extraction protocols for the quantification of phycobilins in aqueous phytoplankton extracts. *J. Appl. Phycol.* 23:865–71.

Laza-Martínez, A. 2012. *Urgorri complanatus* gen. et sp. nov. (Cryptophyceae), a red-tide-forming species in brackish waters. *J. Phycol.* 48:423–35.

Lovejoy, C., Vincent, W. F., Bonilla, S., Roy, S., Martineau, M.J., Terrado, R., Potvin, M., Massana, R. & Pedrós-Alió, C. 2007. Distribution, phylogeny, and growth of cold-adapted picoprasinophytes in Arctic seas. *J. Phycol.* 43:78–89.

Marquardt, M., Vader, A., Stübner, E. I., Reigstad, M. & Gabrielsen, T. M. 2016. Strong seasonality of marine microbial eukaryotes in a high-Arctic fjord (Isfjorden, in West Spitsbergen, Norway). *Appl. Environ. Microbiol.* 82:1868–80.

Mikkelsen, D. M., Rysgaard, S. & Glud, R. N. 2008. Microalgal composition and primary production in Arctic sea ice: a seasonal study from Kobbefjord (Kangerluarsunnguaq), West Greenland. *Mar. Ecol. Prog. Ser.* 368:65–74.

Novarino, G. 2012. Cryptomonad taxonomy in the 21st century: the first two hundred years. *In* Wolowski, K., Kaczmarska, I., Ehrman, J.E. & Wojta, A.Z. [Eds.] Phycological Reports: Current Advances in Algal Taxonomy and Its Applications: Phylogenetic, Ecological and Applied Perspective. Institute of Botany Polish Academy of Sciences, Kraków, pp. 19–52.

Pančić, M., Hansen, P. J., Tammilehto, A. & Lundholm, N. 2015. Resilience to temperature and pH changes in a future climate change scenario in six strains of the polar diatom *Fragilariopsis cylindrus*. *Biogeosciences* 12:4235–44.

Paulsen, B. S., Vieira, A. A. H. & Klaveness, D. 1992. Structure of extracellular polysaccharides produced by a soil *Cryptomonas* sp. (Cryptophyceae). *J. Phycol.* 28:61–3.

Potvin, M. & Lovejoy, C. 2009. PCR-based diversity estimates of artificial and environmental 18S rRNA gene libraries. *J. Eukaryot. Microbiol.* 56:174–81.

Poulin, M., Daugbjerg, N., Gradinger, R., Ilyash, L., Ratkova, T. & von Quillfeldt, C. 2011. The pan-Arctic biodiversity of marine pelagic and sea-ice unicellular eukaryotes: a first-attempt assessment. *Mar. Biodivers.* 41:13–28.

Pringsheim, E. G. 1944. Some aspects of taxonomy in the Cryptophyceae. *New Phytol.* 43:143–50.

Pringsheim, E. G. 1968. Zur Kenntnis der Cryptomonaden des Süßwassers. *Nova Hedwigia* 16:367–401.

Raho, N., Jaén, D., Mamán, L., Rial, P. & Marín, I. 2014. psbA based molecular analysis of cross-feeding experiments suggests that *Dinophysis acuta* does not harbour permanent plastids. *Harmful Algae* 35:20–8.

Ronquist, F. & Huelsenbeck, J. P. 2003. MrBayes 3: Bayesian phylogenetic inference under mixed models. *Bioinformatics* 19:1572–4.

Roy, S., Llewellyn, C. A., Egeland, E. S. & Johnsen, G. 2011. *Phytoplankton Pigments: Characterization, Chemotaxonomy and Applications in Oceanography*. Cambridge University Press, Cambridge, 845 pp.

Shiratori, T. & Ishida, K. 2016. A new heterotrophic cryptomonad: *Hemiarma marina* n. g., n. sp. *J. Eukaryot. Microbiol.* 63:804–12.

Sørensen, N., Daugbjerg, N. & Gabrielsen, T. M. 2012. Molecular diversity and temporal variation of picoeukaryotes in two Arctic fjords, Svalbard. *Polar Biol.* 35:519–33.

Stecher, A., Neuhaus, S., Lange, B., Frickenhaus, S., Beszteri, B., Kroth, P. G. & Valentin, K. 2016. rRNA and rDNA based assessment of sea ice protist biodiversity from the central Arctic Ocean. *Eur. J. Phycol.* 51:31–46.

Šupraha, L., Bosak, S., Ljubešić, Z., Mihanović, H., Olujić, G., Mikac, I. & Viličić, D. 2014. Cryptophyte bloom in a Mediterranean estuary: high abundance of *Plagioselmis* cf. *prolonga* in the Krka River estuary (eastern Adriatic Sea). *Sci. Mar.* 78:329–38.

Swofford, D. L. 2002. PAUP* Phylogenetic Analysis Using Parsimony (*and Other Methods), Version 4.0b10. Sinauer Associates, Sunderland, Massachusetts.

Vallières, C., Retamal, L., Ramlal, P., Osburn, C. L. & Vincent, W. F. 2008. Bacterial production and microbial food web structure in a large arctic river and the coastal Arctic Ocean. *J. Mar. Syst.* 74:756–73.

Vehmaa, A. & Salonen, K. 2009. Development of phytoplankton in Lake Pääjärvi (Finland) during under-ice convective mixing period. *Aquat. Ecol.* 43:693–705.

Waterhouse, A. M., Procter, J. B., Martin, D. M. A., Clamp, M. & Barton, G. J. 2009. Jalview Version 2-A multiple sequence alignment editor and analysis workbench. *Bioinformatics* 25:1189–91.

Zapata, M., Rodríguez, F. & Garrido, J. L. 2000. Separation of chlorophylls and carotenoids from marine phytoplankton: a new HPLC method using a reversed phase C_8 column and pyridine-containing mobile phase. *Mar. Ecol. Prog. Ser.* 195:29–45.

Supporting Information

Additional Supporting Information may be found in the online version of this article at the publisher's web site:

Figure S1. Standard curve used for calculating cell densities of *Baffinella frigidus* in the temperature and salinity experiments based on Raw Fluorescence Units (RFU) measurements. Counted cell densities were plotted as a function of RFU and linear regression was used to get the relationship between cell densities and RFU.

Figure S2. Standard curves used for calculating cell densities of *Baffinella frigidus* in the light experiments based on Raw Fluorescence Units (RFU) measurements. Counted cell densities were plotted as a function of RFU and linear regression was used to get the relationship between cell densities and RFU.

Figure S3. Chloroplast color of *Baffinella frigidus* grown at different light intensities. (A, B) Red colored cells grown at 5 μmol photons $\cdot$ m^{-2} $\cdot$ s^{-1}. (C) Concentrated cell suspension in Falcon tube revealing a dense red color. (D, E) Green colored cells grown at 100 μmol photons $\cdot$ m^{-2} $\cdot$ s^{-1}. (F) Dense culture in Nunc flask grown at 100 μmol photons $\cdot$ m^{-2} $\cdot$ s^{-1}.

Figure S4. Semi-log plots of calculated cell densities from the temperature experiments of *Baffinella frigidus* as a function of days. The periods used (d) for calculating growth rates during exponential growth are indicated by bold colored lines (three replicates A, B, and C). No exponential growth was achieved at 10°C and is therefore it is not included.

Figure S5. Semi-log plots of calculated cell densities from the salinity (5, 10, 15, 20, 25, and 30) experiments of *Baffinella frigidus* as a function of days. The periods used (d) for calculating growth rates during exponential growth are indicated by bold colored lines (three replicates A, B, and C).

Figure S6. Semi-log plots of calculated cell densities from the light (5, 20, 40, 60, 80, and 100 μmol photons $\cdot$ m^{-2} $\cdot$ s^{-1}) experiments of *Baffinella frigidus* as a function of days. The periods used (d) for calculating growth rates during exponential growth are indicated by bold colored lines (three replicates A, B, and C).